The chemoenzymatic synthesis of glycan-terminated oligo(Leu)x

Sarah P. Black [iD] [1], Melinda Liu [2], Cesar Castillo [1], Wynne Coradeli [1], Filbert Totsingan [1], Cody B. Edson [1], Sagar D. Khare [2] and Richard A. Gross [iD] [1]*

[1]New York State Center for Polymer Synthesis, Department of Chemistry and Chemical Biology, Rensselaer Polytechnic Institute, Troy, NY, United States, [2]Chemistry and Chemical Biology, Rutgers University, Newark, NJ, United States

Introduction: Glycopeptides contain carbohydrate moieties (glycans) covalently attached to the side chain and/or terminal peptide units. Since glycans are present on cell surfaces, these constructs can potentially address a wide array of therapeutic functions. To overcome the deficiencies associated with current synthetic routes to glycopeptides, such as costly processes and toxic reagents, this work aimed to develop versatile environmentally friendly protease-catalyzed peptide synthesis routes to peptides decorated with a glycan at their N-terminus.

Methods: "Grafters" were first synthesized that consist of a glycan conjugated directly, or through a spacer, to the amine group of L-Phe-ethyl ester (Phe-OEt). The role of Phe-OEt is to increase the conjugate's recognition by the protease (papain) catalytic active site. A series of grafters were synthesized with variation of the glycan structure, linkage-chemistry, and presence of an oligo (ethylene glycol) "spacer" of varied length between the glycan and Phe-OEt moiety. High grafter efficiency will result by the successful acceptance of the grafter at the enzymes S1/S2 subsites, formation of an acyl enzyme complex and subsequent conversion to glycan-terminated oligo(Leu)x (x ≥ 1), as opposed to construction of non-glycan N-terminated oligo(Leu)x.

Results and discussion: While glycan-Phe-OEt grafters without a spacer between the glycan and Phe-OEt resulted in low grafter efficiency (8.3% ± 2.0%), insertion of a short oligo (ethylene glycol) spacer between the glycan and Phe-OEt moieties (glycan-PEGn-Phe-OEt, $n \geq 3$) increased the grafter efficiency by 3-fold−24.5% ± 1.8%. In addition, computational modeling was performed using Rosetta software provided insights on a molecular level of how grafter efficiency is influenced by the PEG spacer length.

1 Introduction

Glycopeptides are bioconjugates that exploit the properties of glycans and peptides in a synergistic manner. The glycosylation of peptides provides advantageous properties for a variety of applications. For example, cationic peptides containing 5–30 amino acid residues can function as cell-penetrating peptides (CPPs) (Derakhshankhah and Jafari, 2018). CPPs cross cell membranes to deliver cargo with important bioactivity; however, issues related to CPPs include non-selective delivery to specific cellular components or cell types, as well as their potential toxicity (Dutot et al., 2010; Gallego et al., 2019). Studies have demonstrated
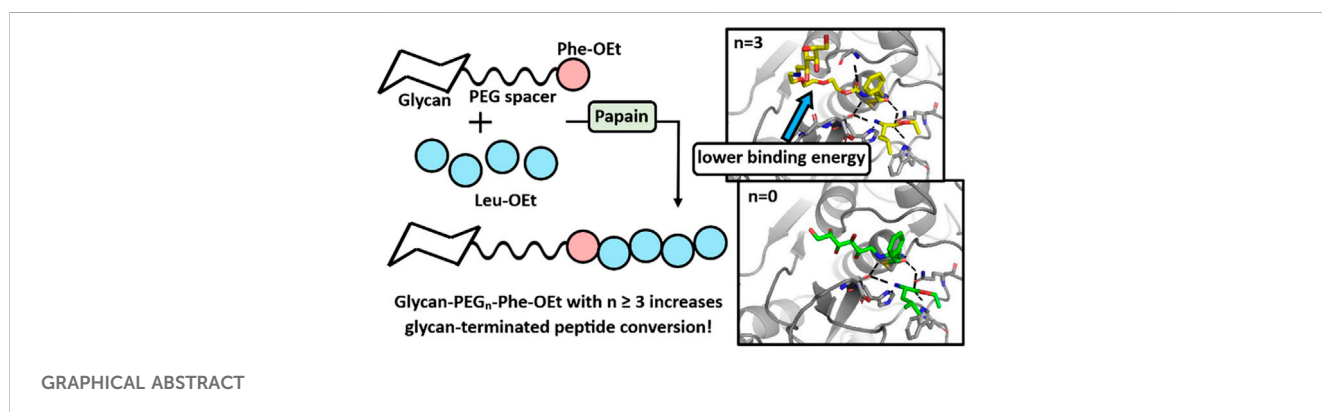
that the glycosylation of CPPs results in improved uptake efficiency as well as a reduction in their toxicity (Dutot et al., 2010; Gallego et al., 2019). More generally, terminally-glycosylated peptides have improved bioavailability, absorption and organ retention compared to their non-glycosylated counterparts (Bapst et al., 2009; Moradi et al., 2013). For example, a galactose-modified peptide at its C-terminus exhibited longer retention in the kidney compared to the non-glycan terminated peptide (Bapst et al., 2009; Moradi et al., 2013). In addition, the conjugation of various carbohydrates at the N-terminus led to improved peptide stabilization against digestion by enzymes, and provided increased cell permeation and absorption (Moradi et al., 2013).
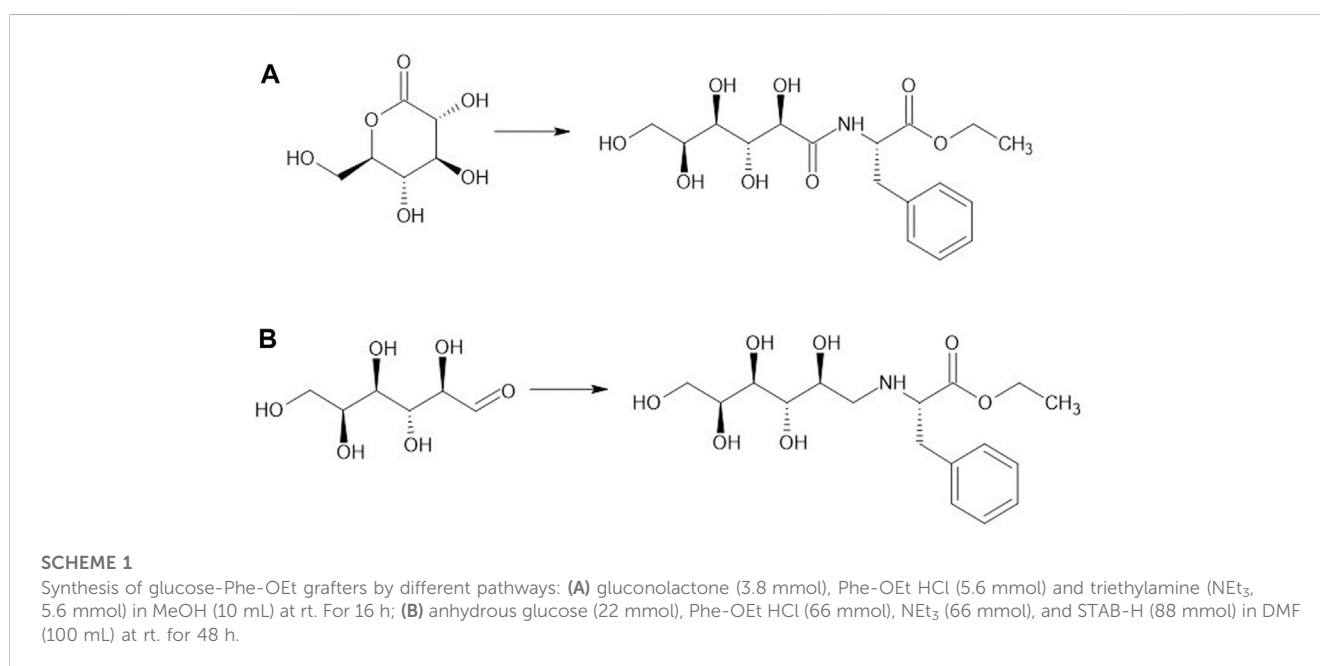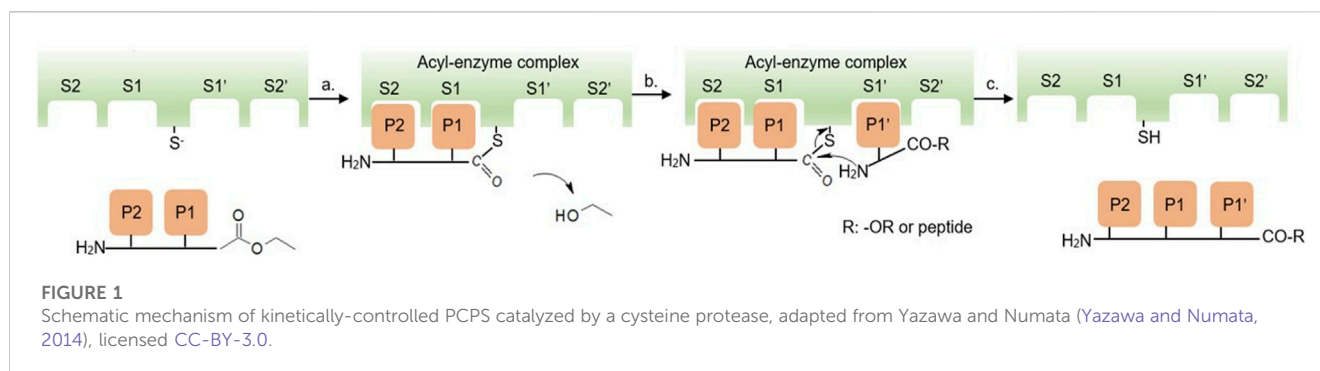
The ability of peptides to self-assemble provides valuable properties, such as stimuli responsiveness, for use as drug delivery vehicles (Jain et al., 2012; Fan et al., 2017). Glycosylation of peptide drug delivery vehicles can improve their selectivity for targeted tissues and cells, modulate release rates, and enable their use as oral delivery formulations (Jain et al., 2012). For example, glycan-terminated carriers can undergo successful recognition by lectin receptors, which are carbohydrate-binding moieties present at cell surfaces (Jain et al., 2012). Lectin receptor recognition allows glycosylated-peptides to function as selective drug delivery vehicles (Jain et al., 2012). In addition, glycosylation of carriers can improve their ability to function as oral drug delivery agents (Pukanud et al., 2009). For example, mannosylated liposomes encapsulating acyclovir increased *in vitro* drug absorption due to the presence of mannose (Pukanud et al., 2009). Also, conjugating glycans to carriers can be used to increase drug release rates. Examples include dextran-conjugated PPI dendrimers, which achieved a higher sustained release of doxorubicin (anti-cancer drug) compared to free doxorubicin (Agarwal et al., 2009; Jain et al., 2012).

Given that glycopeptides serve important functions for a myriad of biomedical applications, the ability to synthesize these molecules by an environmentally friendly route that would make them available to a larger population of patients, including those of underprivileged individuals and in developing nations, would be highly impactful to their potential benefit to a broader patient group. Currently, the dominant synthetic route to prepare relatively short peptides (3–15 amino acids) is by using solid phase peptide synthesis (SPPS) (Kajihara et al., 2010). SPPS involves a solid support resin, from which peptides are grown via stepwise protection-deprotection chemistry (Stawikowski and Fields, 2012; Duro-Castano et al., 2014). While SPPS provides precise control of peptide sequence and length, its repetitive use of protection-deprotection chemistry leads to tedious and expensive processes that have poor atom economy due to the generation of toxic by-products and solvents (Bordusa, 2002). In addition to SPPS, another frequently used peptide synthetic method that provides relatively longer chains (>200 residues) is N-carboxyanhydride ring-opening polymerization (NCA-ROP) (Deming, 2012). However, NCA-ROP requires protection of the carbohydrate hydroxyl moieties, is not useful to prepare peptides of controlled sequence, requires hazardous reagents such as phosgene as well as high purity monomers and strictly controlled reaction conditions (e.g., exclusion of water) (Hadjichristidis et al., 2009; Deming, 2012). Furthermore, both SPPS and NCA-ROP necessitate the use of reagents classified as problematic by REACH (Registration, Evaluation, Authorization and Restriction of Chemicals) and other regulatory agencies (Martin et al., 2020). Although there have been recent work into more sustainable approaches to the traditional SPPS, such as liquid-phase peptide synthesis (LPPS), there are still issues in achieving methods that are truly environmentally friendly. This work explores for the first time the potential use of protease-catalyzed peptide synthesis (PCPS), as an environmentally sustainable alternative, to synthesize glycopeptides.

Kinetically controlled PCPS is conducted in aqueous media, catalyzed by serine proteases and converts amino acid (AA) ethyl ester (NH_2-AA-OEt) monomers to oligomers (Qin et al., 2011). Subsites S and S′ are located in the protease active site region as illustrated in Figure 1. The acyl donor has an activated ester moiety at its C-terminus. Suitable acyl donor substrates are recognized, positioned, and activated at the protease S1/S2 subsites by nucleophilic attack by the cysteine protease thiol group at the ester carbonyl C-terminus to form the covalent acyl-enzyme activated complex and ethanol is the leaving group (*step a* in Figure 1). (Erez et al., 2009) The acyl donor structure is very important in this step since its structural features, and those at the S1/S2 subsites, determine whether there is productive binding and acyl-enzyme bond formation. After successful formation of the acyl-enzyme complex, an incoming nucleophile that, for peptide bond formation, is a NH_2-AA-OEt monomer or, potentially, NH_2-$(AA)_n$-OEt where n ≥ 1, binds at the S1′/S2′ subsites such that the amine-terminus is positioned to perform a nucleophilic attack at the carbonyl of the acyl-enzyme

GRAPHICAL ABSTRACT

FIGURE 1
Schematic mechanism of kinetically-controlled PCPS catalyzed by a cysteine protease, adapted from Yazawa and Numata (Yazawa and Numata, 2014), licensed CC-BY-3.0.

SCHEME 1
Synthesis of glucose-Phe-OEt grafters by different pathways: **(A)** gluconolactone (3.8 mmol), Phe-OEt HCl (5.6 mmol) and triethylamine (NEt$_3$, 5.6 mmol) in MeOH (10 mL) at rt. For 16 h; **(B)** anhydrous glucose (22 mmol), Phe-OEt HCl (66 mmol), NEt$_3$ (66 mmol), and STAB-H (88 mmol) in DMF (100 mL) at rt. for 48 h.
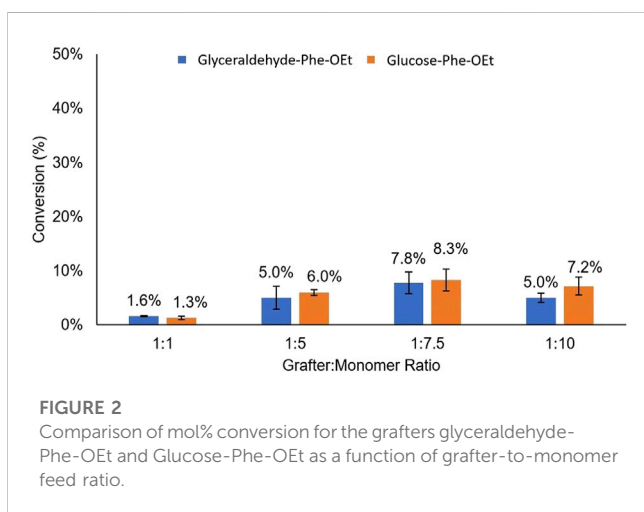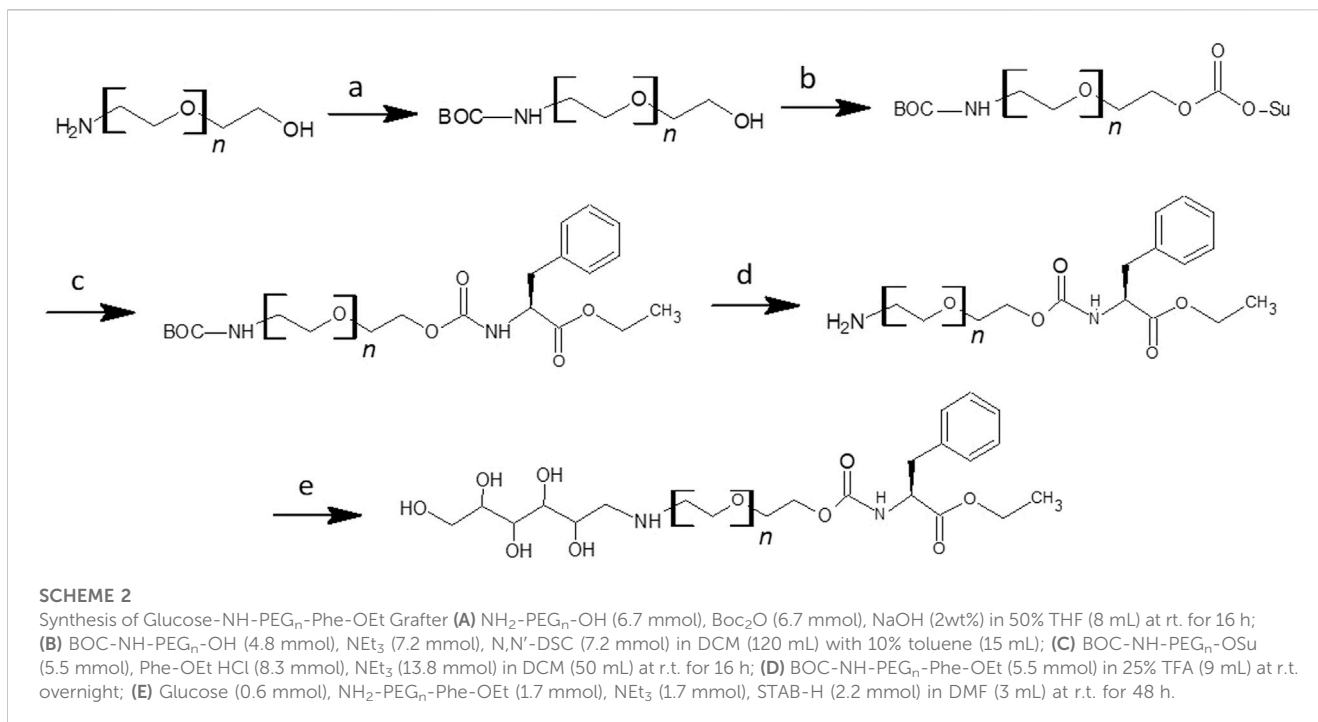
complex and peptide formation occurs with regeneration of the cysteine thiol group (*step b and c*, Figure 1). Concurrent extension of the peptide chain can then occur as the new C-terminal ester group is displaced by formation of an acyl-enzyme complex and another N-terminal amine functionality of an incoming substrate (i.e., NH$_2$-(AA)$_n$-OEt) results in chain elongation. This results in the growth of peptide chains to form homopeptides, co-peptides, alternating, and block copeptides (Bordusa, 2002; Viswanathan et al., 2010; Qin et al., 2011; Yazawa and Numata, 2014).

The first known synthesis of a peptide-polymer conjugate by PCPS was recently reported by our group (Centore et al., 2020). PCPS was used to form *in-situ* self-assembling diblock copolymers consisting of a poly (ethylene glycol), PEG, and oligoleucine, oligo(Leu)$_x$, segment. For diblock formation to occur, the monomethoxy-PEG-Phe-OEt segment must form an acyl-enzyme complex at a rate that effectively competes with oligo(Leu)$_x$ homo-oligopeptide synthesis. In other words, monomethoxy-PEG-Phe-OEt must be suitably positioned at the papain active site to form an acyl-enzyme complex that reacts with NH$_2$-(Leu)$_x$-OEt (x ≥ 1) at a

similar or faster rate than formation of oligo(Leu)$_x$ homo-oligopeptide. This occurred, resulting in a coproduct mixture consisting of mPEG$_{45}$-*b*-Phe(Leu)$_x$ and oligo(Leu)$_x$.

Towards the *in-situ* formation of glycopeptides, this study explores whether glycan-Phe-OEt can function similarly to monomethoxy-PEG-Phe-OEt. Unlike PEG where hydroxyl groups are restricted to the chain ends, glycans present multiple hydroxyl groups with specific stereochemical features. Herein, we evaluate how the glycan structure and its proximity to the active site influences its ability to function as an effective grafter during PCPS using papain and Leu-OEt as the protease and monomer, respectively. Variables interrogated include the molar ratio of grafter to monomer, the glycan structure, the glycan-peptide conjugate chemistry, and the systematic variation in the length of an ethylene glycol spacer to decrease glycan S1/S2 subsite interactions. Products and starting materials were characterized by MALDI-TOF and NMR spectroscopy. In addition, computational modeling was performed using Rosetta software to gain insights on a molecular level of how grafter efficiency is influenced by the PEG spacer length.

SCHEME 2
Synthesis of Glucose-NH-PEGn-Phe-OEt Grafter **(A)** NH₂-PEGn-OH (6.7 mmol), Boc₂O (6.7 mmol), NaOH (2wt%) in 50% THF (8 mL) at rt. for 16 h;
(B) BOC-NH-PEGn-OH (4.8 mmol), NEt₃ (7.2 mmol), N,N'-DSC (7.2 mmol) in DCM (120 mL) with 10% toluene (15 mL); **(C)** BOC-NH-PEGn-OSu
(5.5 mmol), Phe-OEt HCl (8.3 mmol), NEt₃ (13.8 mmol) in DCM (50 mL) at r.t. for 16 h; **(D)** BOC-NH-PEGn-Phe-OEt (5.5 mmol) in 25% TFA (9 mL) at r.t.
overnight; **(E)** Glucose (0.6 mmol), NH₂-PEGn-Phe-OEt (1.7 mmol), NEt₃ (1.7 mmol), STAB-H (2.2 mmol) in DMF (3 mL) at r.t. for 48 h.

FIGURE 2
Comparison of mol% conversion for the grafters glyceraldehyde-
Phe-OEt and Glucose-Phe-OEt as a function of grafter-to-monomer
feed ratio.

2 Results and discussion

2.1 Glycan-Phe-OEt grafter synthesis

Studies were performed to probe how glycan-AA-OEt structure influences its ability to function as an effective grafter, that productively binds at the S1/S2 subsites to form an acyl-enzyme complex and subsequently reacts with the amino-terminus of $(AA)_x$-OEt ($x \geq 1$) to form a glycopeptide conjugate. First, the structure of the linkage between glucose and NH₂-Phe-OEt was varied. The synthetic route of glucolactone ring-opening by the amine of NH₂-Phe-OEt resulted in amide bond formation (glucose-$C=O$-NH-Phe-OEt) whereas, to prepare the CH_2-NH-linked grafter (glucose-CH_2-NH-Phe-OEt), anhydrous glucose was reacted with NH₂-Phe-OEt HCl using NEt₃ as the base followed by treatment of the reducing agent sodium

triacetoxyborohydride, STAB-H (Schemes 1A, B, respectively). The selection of STAB-H in place of sodium cyanoborohydride was motivated by that the former is a safer and more environmentally friendly reducing agent (Abdel-Magid and Mehrman, 2006). The identical procedure was also performed with glyceraldehyde as described in the experimental section to obtain glyceraldehyde-CH_2-NH-Phe-OEt. The successful synthesis of these compounds was confirmed by NMR and ESI-MS. The ^1H NMR of each grafter, displayed in Supplementary Figures S1–S3, show that the NMR signals and corresponding integration values are consistent with that of the expected products. In addition, theoretical molecular weights correspond to molecular weights determined using ESI-MS, as shown in Supplementary Figures S8–S10. The grafters were utilized in papain-catalyzed co-oligomerizations with Leu-OEt. The feed ratio of the glycan grafter to Leu-OEt monomer was varied and those experiments are described below in Section 1.3.

2.2 Glycan-PEGn-Phe-OEt grafter synthesis

In addition to grafters synthesized by covalent attachment of glucose and Phe-OEt, grafters were also synthesized where these two moieties were separated by short PEG spacers that varied in length from 1 to 4 repeat units. To synthesize glucose-NH-PEGn-Phe-OEt grafters, amino-PEGn-OH (n = 1,2,3,4) was reacted with di-tert-butyl dicarbonate (boc anhydride) under alkaline conditions (Scheme 2A). The tert-butyloxycarbonyl (boc) protected amino-PEGn-OH was then treated with N,N'-Disuccinimidyl carbonate (N,N'-DSC) using triethylamine as a proton acceptor to form the corresponding N-hydroxysuccinimide intermediate (Scheme 2B). The activated carbonate was then treated with Phe-OEt HCl, under alkaline conditions, to conjugate Boc-amino-PEGn-O-Su and Phe-OEt via formation of a carbamate bond (Scheme 2C). The product
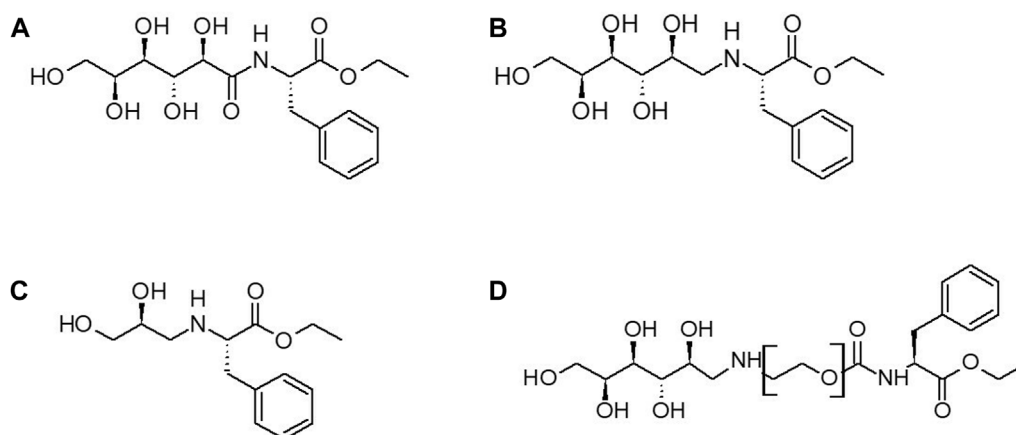
FIGURE 3
Structures of Glycan Grafters: **(A)** glucose-*C=O-NH*-Phe-OEt **(B)** glucose-*CH₂-NH*-Phe-OEt grafter **(C)** glyceraldehyde-*CH₂-NH*-Phe-OEt **(D)** Glucose-PEG_n-*O-C=O-NH*-Phe-OEt.
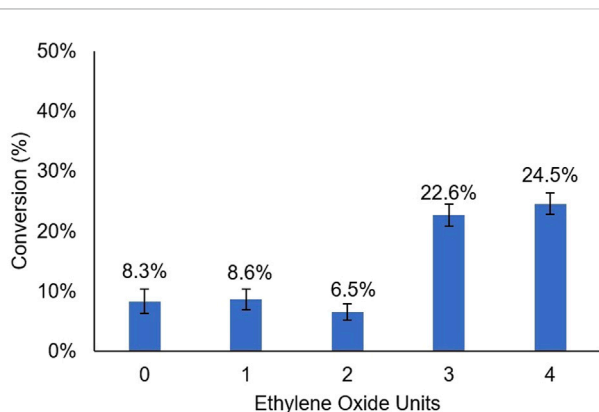

FIGURE 4
Grafter Conversion Based on PEG Spacer Length: Mole percent conversion from grafters Glucose-PEG$_n$-*O-C=O-NH*-Phe-OEt, with n = 1, 2, 3, 4, to glycan-terminated peptides. The grafter to monomer ratio is 1:7.5.

was de-protected (Scheme 2D), forming amino-PEG$_n$-Phe-OEt, that has a free amine that underwent a reductive amination with glucose using STAB-H as the reducing agent (Scheme 2E). The successful synthesis of these compounds was confirmed by NMR and ESI-MS. The ¹H NMR of the glucose-PEG$_n$-Phe-OEt grafter, displayed in S6, shows NMR signals and corresponding integration values consistent with those expected for the product. In addition, theoretical molecular weights correspond to molecular weights determined using MALDI-TOF analysis (see S11). As above, the grafters were utilized in papain-catalyzed co-oligomerizations with Leu-OEt monomer.

2.3 Analysis of grafter efficiency

Herein, the grafter efficiency is defined as the percent of moles of grafter converted to moles of N-terminal glycan functionalized oligopeptide (mol%). Analysis of grafter efficiency was determined by ¹H-NMR peak integration of the product precipitate, provided in Supplementary Figure S12, in combination with MALDI-TOF data of the product precipitate, as seen in Supplementary Figure S13. From the ¹H-NMR spectrum of the precipitate, the mole ratio of N-terminal glycan oligopeptide to non-glycan terminated oligopeptide was determined by dividing the average integration of the glycan-terminated aromatic proton signal at ~7.2 ppm by the average integration of the β-proton signal at ~4.5 ppm of the non-glycan terminated oligopeptide (Supplementary Equation S1). This gives the mol% of both glycan-terminated oligopeptide and non-glycan terminated oligopeptide in the product mixture (Supplementary Equation S2). The weight percent, wt%, of glycan-terminated and non-glycan terminated oligopeptide in the product mixture was then determined (Supplementary Equations S3, S4). The actual mass of glycan-terminated oligopeptide present in the product precipitate was then calculated by multiplying its wt% by the total precipitate mass measured (Supplementary Equation S5). The mass of glycan-terminated oligopeptide was then converted to moles based on the product's molecular weight, using the average degree of polymerization (DP) of the Leu$_x$ in the oligopeptide, determined by MALDI-TOF (Supplementary Equation S6). Finally, the percent conversion of grafter to glycan-terminated grafter was calculated by dividing the moles of the glycan-terminated oligopeptide by the starting moles of the grafter (Supplementary Equation S7).

2.4 Influence of grafter structure

The glucose-*CH₂-NH*-Phe-OEt and glucose-*C=O-NH*-Phe-OEt present amine and amide linker groups, respectively, that may have different affinities at the S1/S2 subsites. At the molar ratio of 1: 5 grafter-to-Leu-OEt, mol% conversions of these grafters to glycan terminated peptides were both low (6.0% ± 0.5% and 3.9% ± 0.4 %, respectively). The slightly higher value obtained with the *CH₂-NH* linker may be a due to the lower bond flexibility of the *C=O-NH*

TABLE 1 Energies of the pockets in each Glucose-NH_2-PEG_n-Phe-OEt grafter model and standard deviations among 100 decoys per model in REU (Rosetta Energy Units). Pockets were defined by the grafter, the monomer, the catalytic residues, and residues neighboring the grafter and monomer.

Ethylne oxide units in grafter	Pocket Energy (REU)	Standard Deviation (REU)
0	−24.5	0.3
1	−25.8	0.0
2	−25.9	0.0
Average	−25.4	
3	−28.6	0.8
4	−28.5	0.0
Average	−28.6	

TABLE 2 Total energies and van der Waals attractive energies between the substrates in each Glucose-NH_2-PEG_n-Phe-OEt grafter model and standard deviations among 100 copies per model in REU (Rosetta Energy Units).

| Ethylne oxide units in grafter	Total substrates energy		vdW attraction between the substrates	
	Energy (REU)	Standard Deviation (REU)	Energy (REU)	Standard Deviation (REU)
0	0.5	0.16	−2.3	0.0
1	0.1	0.0	−2.2	0.0
2	−0.2	0.0	−2.3	0.0
Average	0.1		−2.3	
3	−0.5	0.5	−3.0	0.1
4	−0.6	0.0	−2.8	0.0
Average	−0.6		−2.9	

linker, although it could also be related to negative interactions between subsite residues and the amide moiety. Glucose-CH_2-NH-Phe-OEt consists of a 6-carbon sugar that presents five hydroxyl groups. To probe whether higher grafter efficiency would result by use of a smaller glycan, the 3-carbon oxidized polyol glyceraldehyde was coupled to Phe-OEt by reductive amination, resulting in glyceraldehyde-CH_2-NH-Phe-OEt (See Scheme 1C).

Figure 2 compares the mol% grafter conversion efficiency of Glucose-CH_2-NH-Phe-OEt and glyceraldehyde-CH_2-NH-Phe-OEt using papain and Leu-OEt as catalyst and monomer, respectively. Furthermore, the influence of the monomer-to-grafter ratio was studied for these two grafters. The importance of this variable was established in previous work by our group using $mPEG_{45}$-Phe-OEt (m = methoxy) as grafter and Leu-OEt as monomer for the *in-situ* synthesis of self-assembling $mPEG_{45}$-*b*-Phe(Leu)$_x$ diblock copolymer (Centore et al., 2020). By increasing the monomer-to-grafter feed ratio from 2.5 to 4.1 to 8.2, the grafter conversions increased from 14% ± 0% to 24% ± 1% to 66% ± 4%, respectively. Since the average degree of polymerization of the oligo(Leu)$_x$ segment was about 5.0, it follows that a feed ratio of at least 5 to 1 Leu-OEt to grafter is needed to approach maximum grafter conversion efficiency values.

As illustrated in Figure 2, the grafters Glucose-CH_2-NH-Phe-OEt and Glyceraldehyde-CH_2-NH-Phe-OEt had nearly identical grafter efficiencies across the different grafter-to-monomer ratios. Hence, even with a large decrease in glycan size and number of hydroxyl groups resulting from the substitution of glucose for glyceraldehyde, this strategy did not substantially relieve non-productive interactions between the glycan moieties and the S2 subsite. However, it appears from the small differences in mol % grafter conversion as a function of grafter-to-monomer ratio that there is an apparent maximum at 1:7.5, where 1:1 and 1:7.5 gave the lowest (1.3% ± 0.3%) and highest (up to 8.3% ± 2%) values, respectively. This trend was also observed in our previous work, as discussed above (Centore et al., 2020). Furthermore, the DP of oligo(Leu)$_x$ formed in glucose-Phe-Leu$_x$-OEt conjugates did not significantly change as a function of grafter to monomer feed ratio. In other words, at 1:1, 1:2.5, 1:5, 1:7.5, and 1:10 grafter to monomer ratios, the DP of oligo(Leu)$_x$ formed in conjugates was 2.8 ± 0.2, 3.1 ± 0.5, 2.8 ± 0.1, 2.7 ± 0.2, 2.8 ± 0.2, respectively.

Since both the glucose and glyceraldehyde-derived grafters resulted in similarly low grafter conversions, we then pivoted to an alternative strategy to increase grafter conversion. Specifically, we inserted short PEG spacers of differing lengths between the glycan and Phe-OEt units. Based on our previous studies that reported the preparation of $mPEG_{45}$-*b*-Phe(Leu)$_x$ by PCPS (Centore et al., 2020), it appears that PEG possess structural features that are acceptable by the S1/S2/S3 subsites of papain. Glucose was selected over glyceraldehyde as the glycan since it is larger and, therefore,
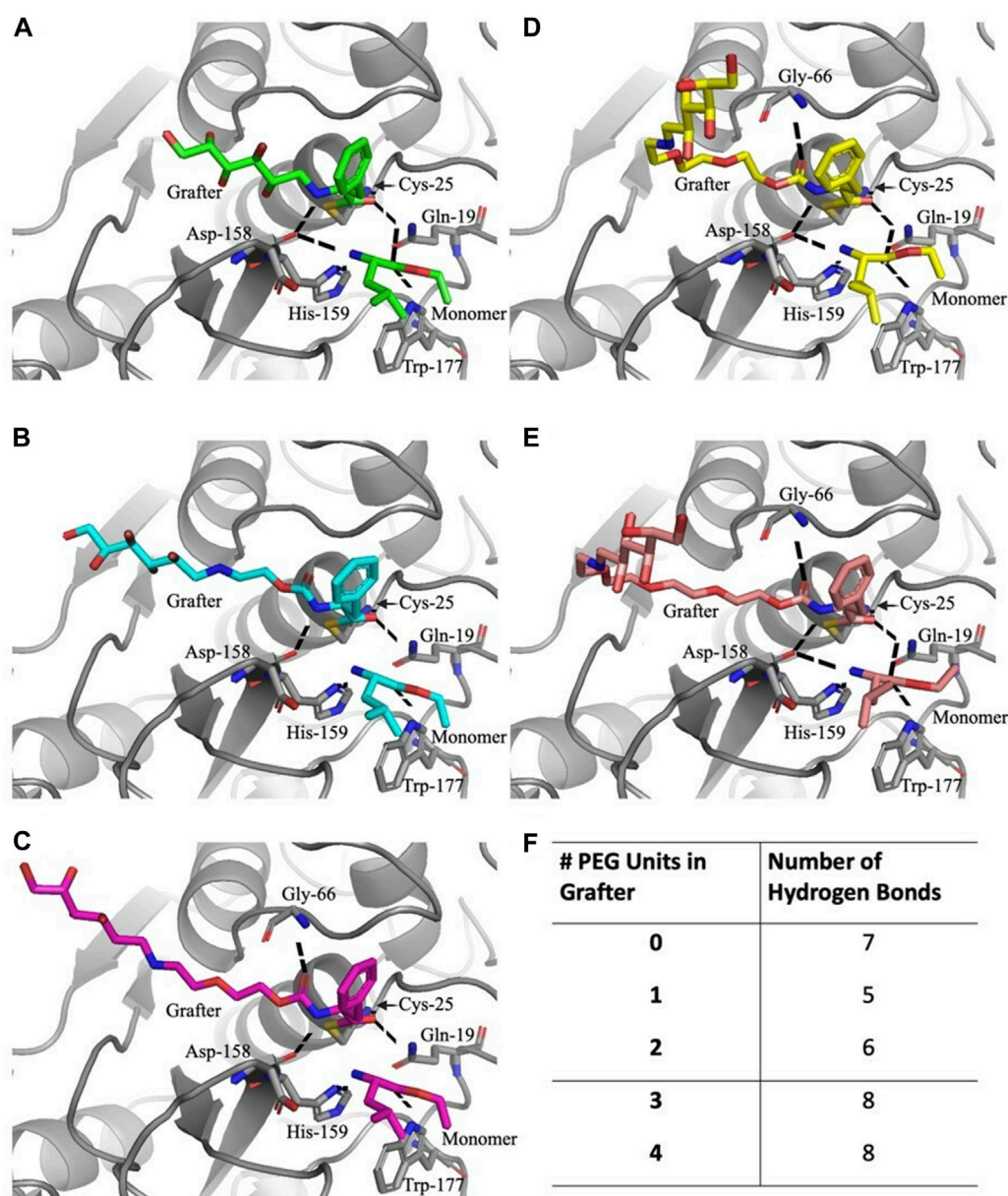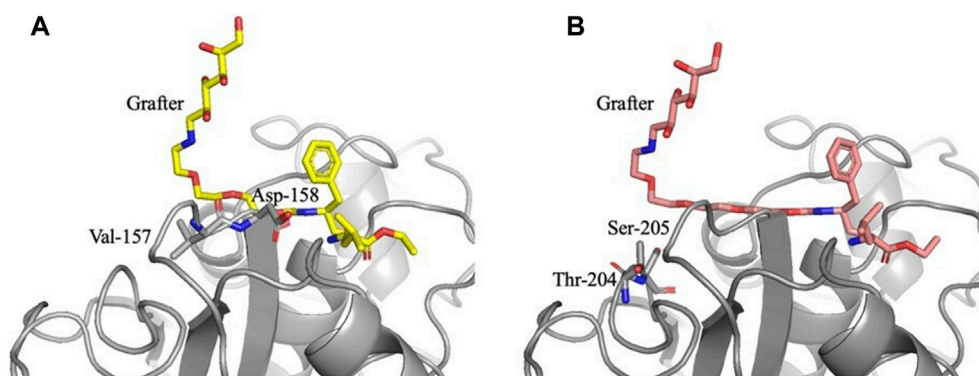
FIGURE 5
Active site docking models with the Glucose-NH$_2$-PEG$_n$-Phe-OEt grafters and hydrogen bonds with the substrates. For the Glucose-NH$_2$-Phe-OEt **(A)** and Glucose-NH$_2$-PEG$_1$-Phe-OEt **(B)** grafters, the five residues that hydrogen bond with the substrates are Gln-19, Cys-25, Asp-158, His-159, and Trp-177. For the Glucose-NH$_2$-PEG$_2$-Phe-OEt **(C)**, Glucose-NH$_2$-PEG$_3$-Phe-OEt **(D)**, and Glucose-NH$_2$-PEG$_4$-Phe-OEt **(E)** grafters, the six residues that hydrogen bond with the substrates are also Gln-19, Cys-25, Gly-66, Asp-158, His-159, and Trp-177. The total number of hydrogen bonds formed with the substrates with each grafter is listed **(F)**.

expected to be more disruptive to recognition at papain S1/S2/S3 subsites. Amino-PEG-OH was selected as the spacer since the grafter mPEG$_{45}$-Phe-OEt was accepted within the papain active site during the synthesis of mPEG$_{45}$-b-Phe(Leu)$_x$ diblock copolymer (Centore et al., 2020). Hence, the new family of grafters are Glucose-NH-PEG$_n$-Phe-OEt with n = 1, 2, 3 and 4 (Figure 3D). By this approach, we sought to determine the minimum spacer length that enables glucose, and presumably other glycan moieties that interact poorly with the S1/S2/S3 subsites, to move sufficiently out of the active site eliminating high energy interactions, resulting in important increases in grafter conversion.

2.5 Effect of spacer addition

The Glucose-NH$_2$-PEG$_n$-Phe-OEt grafter design, where n = 1,2,3,4 were used in subsequent papain-catalyzed reactions at a feed ratio of 1:7.5 grafter-to-Leu-OEt, as this was the optimal feed ratio identified in our previous study (Centore et al., 2020) as well as in Figure 2. As displayed in Figure 4, the presence of a PEG spacer consisting of ≥ 3 ethylene glycol units increased the grafter conversion rate by 3-fold (8.3%–24.5% ± 1.8 %). Smaller PEG spacers with 1 and 2 units gave grafter conversions comparable to the glycan grafter without a PEG spacer. This result indicates

FIGURE 6
Active site docking models with the Glucose-NH$_2$-PEG$_3$-Phe-OEt and Glucose-NH$_2$-PEG$_4$-Phe-OEt grafters and locations of bends. For the Glucose-NH$_2$-PEG$_3$-Phe-OEt grafter **(A)**, the bend is located near Val-157 and Asp-158. For the Glucose-NH$_2$-PEG$_4$-Phe-OEt grafter **(B)**, the bend is located near Thr-204 and Ser-205.

there is a critical distance required to move the glycan from the active site and thereby relieve negative interactions. The DP of oligo(Leu)$_x$ formed in glucose-PEG$_n$-Phe-OEt conjugates did not significantly differ based on presence or length of PEG spacer. The DP of oligo(Leu)$_x$ in conjugates with Glucose-PEG$_n$-O-C=O-NH-Phe-, where n = 1,2,3,4 was 2.0 ± 0.0, 1.72 ± 0.2, 2.2 ± 0.5, 2.8 ± 0.1, respectively.

Based on our previous report (Centore et al., 2020), a PEG chain length of about 45 units (methoxy-PEG$_{45}$-Phe-OEt) is expected to be sufficient to increase the grafter conversion to 66% at a monomer-to-grafter ratio of 8.2. Hence, it is likely that further increases in the PEG chain spacer length will result in higher %-grafter values.

2.6 Rationalizing observed PEG spacer length preferences using computational modeling

To investigate the greater conversion of grafters with longer PEG spacers as compared to grafters with shorter PEG spacers, computational modeling was performed using Rosetta software. Acyl-enzyme models were generated using the Leu-OEt monomer as the acyl-acceptor for each of the Glucose-NH$_2$-PEG$_n$-Phe-OEt grafters as the acyl-donors, where n = 0,1,2,3,4. The acyl-acceptor is represented as a Leu-OEt monomer but may exist as short [Leu]$_x$-OEt oligomers.

Computed pocket energies and first-shell interactions were used as proxies for activity. Catalytically active models were generated constraining a near-attack geometry between the acyl-enzyme intermediate and the attacking nucleophile for peptide bond formation. Lower pocket energies would represent more stable pockets, which may translate to more active pockets. The pocket energies can be separated into two clusters. The models with the longer grafters, with an average of −28.6 REU, have lower pocket energies than the models with the shorter grafters, with an average of −25.4 REU, which is consistent with the experimental data indicating that longer grafters having greater grafter conversion. (Table 1).

Therefore, the modeling was able to generate structures that align with the experimental data.

As the experimental data demonstrated, grafters with larger PEG spacers had higher graft efficiencies than those with smaller or no PEG spacers. To better understand the molecular origins of this result, total energies and van der Waals attractive energies between the substrates in each Glucose-NH$_2$-PEG$_n$-Phe-OEt grafter model was determined. Breakdown of individual energies of each residue in the pocket reveals that the combined energies of the grafter and monomer decrease as the PEG spacer length increases (Table 2). This suggests that the substrates themselves are more stable with the longer grafters. This observation aligns with the accompanying increase in the number of hydrogen bonds that the substrates engage in with the pockets as the grafter spacer length increases (Figure 5).

Of the favorable residue interactions that stabilize the substrate positions in the active sites, all the models share 5 common hydrogen bonds (Figure 5): the carbonyl oxygen on the grafter is coordinated with the side chain amide nitrogen on Gln-19 and with the backbone nitrogen on Cys-25. The nitrogen on the grafter hydrogen bonds with the backbone carbonyl oxygen on Asp-158. Meanwhile, the monomer unit is stabilized through its amine nitrogen to the Δ-nitrogen on His-159 and its carbonyl oxygen to the side chain amine nitrogen on Trp-177 (Figure 5B). The substrates in the model with the grafter with 2 PEG units are stabilized with an additional hydrogen bond to Gly-66 (Figure 5C). The grafter is further stabilized with a hydrogen bond between the ester carbonyl oxygen and the backbone nitrogen on Gly-66. The model with the grafter without the PEG spacer lacks the hydrogen bond between the grafter and Gly-66, but the monomer is positioned in such a way that allows for hydrogen bonding between the carbonyl oxygen and the side chain amide nitrogen on Gln-19 and between the nitrogen and the backbone carbonyl oxygen on Asp-158 (Figure 5A). This grafter itself is the shortest of the five, which limits how many residues it is capable of interacting with, as seen with the lack of the hydrogen bond with Gly-66 due to the geometry and lack of the pre-linker

carbonyl oxygen. As for the models with the grafters with 3 and 4 PEG units, the substrates make 8 total hydrogen bonds. In addition to the common 5, both grafters are able to hydrogen bond with Gly-66, like the grafter with 2 PEG units, and both monomers are able to hydrogen bond to Gln-19 and Asp-158, like the monomers with the grafter with 0 PEG units (Figures 5D, E).

Both the grafters with 3 and 4 PEG units curve out and away from the active site, a phenomenon not observed with the other grafters. Interestingly, the two bend at different locations within the pocket. Investigating these bending locations reveals residues that are stabilized by interactions with the bent conformation. The grafter with 3 PEG units bends away from the pocket near Val-157 and Asp-158 (Figure 6A) which have lower energies in models PEG3 grafter than with the shorter grafters. The grafter with 4 PEG units bends away from the pocket near Thr-204 and Ser-205 (Figure 6B) and makes favorable interactions with these residues. The increased freedom of longer grafters to rotate and dock to find the optimal geometry for stabilization in the active site may also allow more optimal fit into the active site. Thus, the docking studies suggest that specific interactions between enzyme and PEG linkers enabled by conformational flexibility in the PEG3 and PEG4 linkers may underlie the observed higher yields with these substrates.

3 Conclusion

Glycan-terminated peptides were successfully synthesized *in situ* by protease-catalyzed peptide synthesis, with glycan-terminated Phe-OEt grafters and Leu-OEt monomers. The amine-linked glucose-Phe-OEt grafter yielded slightly higher glycan-terminated peptide conversion than the amide-linked glucose-Phe-OEt grafter (6.0% ± 0.5% and 3.9% ± 0.4 %, respectively) perhaps due to the increased mobility of the amine bond in comparison to the more rigid amide bond. Through a feed ratio study, it was shown that the ratio of glycan grafter (glucose-Phe-OEt, glyceraldehyde-Phe-OEt) to Leu-OEt monomer did impact conversion rates, and the highest grafter efficiency, 8.3% ± 2%, was achieved at a ratio of 1:7.5 grafter-to-monomer. Overall, the conversion of glycan-Phe-OEt grafter to glycan-terminated peptide was <10%; indicating that the glycan grafter reacts with Leu-OEt monomer at a much slower rate than Leu$_x$-OEt homopeptide formation. To mitigate the low glycan-terminated peptide conversion, glucose grafters were synthesized with a PEG$_n$ spacer (n = 1,2,3,4) between the glycan and Phe-OEt moiety in the hopes of reducing unfavorable binding interactions of the glycan at the protease active site. The presence of a PEG$_n$ spacer (n ≥ 3) in the grafters tripled the glycan-terminated conversion, from 8.3% ± 2% to 24.5% ± 1.8%, confirming our hypothesis that the glycan moiety interacts poorly at the protease active site. Limitations of this method include product conversion of ~25% and thus future studies include investigating grafters with longer PEG chain lengths (n > 4) to see if glycopeptide conversion can be further increased. In addition, in this study, glyceraldehyde and glucose were used as model glycans to better understand how glycans interact at the protease active site; however, future studies include investigating more biologically relevant sugars, such as sialyllactose.

4 Experimental

4.1 Materials

L-Leucine ethyl ester hydrochloride (Leu-OEt HCl) and phenylalanine ethyl ester hydrochloride (Phe-OEt HCl) were purchased from Chem Impex. Amino-PEG$_n$-OH (n = 1, 2, 3 and 4) was purchased from Sigma Aldrich and Neta Scientific. Anhydrous glucose and glyceraldehyde were purchased from Sigma Aldrich. Papain was purchased from Acros Organics. High-performance liquid chromatography (HPLC)-grade acetonitrile (ACN), triethylamine (NEt$_3$), diethyl ether (Et$_2$O), toluene, and 99.8% deuterated dimethylsulfoxide (DMSO-d_6) were purchased from Merck Millipore. Methanol (MeOH), dichloromethane (DCM), tetrahydrofuran (THF), dimethylformamide (DMF) and concentrated hydrochloric acid (HCl) were purchased from Fischer Scientific. Anhydrous ethanol (EtOH) was purchased from Koptec. Sodium triacetoxyborohydride (STAB-H) was purchased from Alfa Aesar. Calcium chloride (CaCl$_2$) and magnesium sulfate (MgSO$_4$) were purchased from Avantor. Boc anhydride and N,N′-disuccinimidyl carbonate (N,N′-DSC) was purchased from Chem Impex. All chemicals were purchased in the highest available purity.

4.2 Synthesis of Glycan-Phe-OEt grafter by amidation of gluconolactone

Gluconolactone (0.68 g, 3.8 mmol) was dissolved in MeOH (10 mL) in a 50 mL round bottom flask. Then, Phe-OEt HCl (1.29 g, 5.6 mmol) followed by NEt$_3$ (0.57 g, 5.6 mmol) were added. The reaction was performed for 16 h, at room temperature with magnetic stirring in the presence of air. Thereafter, the reaction solution was added dropwise into 5 °C ether (40 mL) that yielded a precipitate, which was collected and recrystallized in hot EtOH. Solvent removal in a vacuum oven at 40 °C for 16 h yielded 1.13 g (80% yield) of a white powder, with a melting point of 124 °C–126 °C. ^{1}H NMR (600 MHz) chemical shifts (δ in ppm) in DMSO-d_6/10% TFA: 7.77 (d, 1H), 7.21 (dd, 5H), 4.54 (m, 1H), 4.04 (m, 3H), 3.91 (s, 1H), 3.60 (m, 1H), 3.50 (s, 2H), 3.40 (d, 1H), 3,05 (d, 2H), 1.1 (t, 3H); ^{13}C NMR (600 MHz) chemical shifts (δ in ppm) in DMSO-d_6/10% TFA: 172.9, 171.4, 137.5, 130.0, 129.0, 126.9, 73.7, 72.6, 72.0, 70.5, 63.7, 53.4, 37.3. ESI-MS (m/z): [M + H]$^+$ calculated for C$_{17}$H$_{25}$O$_8$N 371.16; found 371.17.

4.3 Reductive amination synthesis of Glycan-Phe-OEt

The glycan (glucose: 3.96 g, 22 mmol; glyceraldehyde: 1.98 g, 22 mmol) was dissolved in 100 mL of DMF (dried over activated molecular sieves) in a 150 mL round bottom flask. Once the glycan was dissolved by gently applying heat, Phe-OEt HCl (15.16 g, 66 mmol) was added, followed by NEt$_3$ (6.68 g, 66 mmol). Finally, STAB-H (18.65 g, 88 mmol) was added to the reaction, and the round bottom flask was capped with a drying tube that contained CaCl$_2$. The reaction was performed at

room temperature for 48 h with magnetic stirring. The protocol for product precipitation and recrystallization was identical to that given above for the synthesis of the glucose-Phe-OEt grafter by amidation of gluconolactone. Solvent removal in a vacuum oven at 40°C for 16 h yielded 4.8 g (81% yield) of a white solid, with a decomposition temperature of 200°C–203°C and 209°C–211°C, for glyceraldehyde-Phe-OEt and glucose-Phe-OEt, respectively. Glucose-Phe-OEt: ^{1}H NMR (600 MHz) chemical shifts (δ in ppm) in DMSO-d_6/10% TFA 7.3 (dd, 5H), 4.1 (m, 1H), 3.8 (m, 3H), 3.6 (m, 3H); ^{13}C NMR (600 MHz) chemical shifts (δ in ppm) in DMSO-d6/10% TFA 130.0, 129.4, 128.9, 128.5, 127.4, 126.8, 60.7, 54.2, 37.2, 35.4, 21.1. ESI-MS (m/z): [M + H]$^+$ calculated for $C_{17}H_{27}O_7N$ 357.19; found 357.19. Glyceraldehyde-Phe-OEt: ^{1}H NMR (600 MHz) chemical shifts (δ in ppm) in DMSO-d6/10% TFA 7.3 (dd, 5H), 4.1 (m, 1H), 3.8 (m, 3H), 3.6 (m, 3H); ^{13}C NMR (600 MHz) chemical shifts (δ in ppm) in DMSO-d_6/10% TFA 130.0, 129.4, 128.9, 128.5, 127.4, 126.8, 60.7, 54.2, 37.2, 35.4, 21.1 ESI-MS (m/z): [M + H]$^+$ calculated for $C_{14}H_{21}O_7N$ 267.15, found 267.15.

4.4 Synthesis of glycan-PEG-Phe-OEt grafter

In a 50 mL round bottom flask, NH_2-(PEG)$_n$-OH (n = 1,2,3,4) (6.7 mmol) was dissolved in 8 mL of a 1:1 (v/v) THF: H_2O. Then, di-tert-butyl dicarbonate (BOC$_2$O, 2.92 g, 6.7 mmol) was added to the solution, followed by 2 weight percent (wt%) NaOH. The reaction was performed at room temperate, with magnetic stirring, in the presence of air. Thereafter, the contents of the reaction flask was added into 30 mL of Et$_2$O, that yielded a precipitate, which was collected by centrifugation and vacuum dried at 40 °C for 16 h. The resulting reaction intermediate, BOC-NH-PEG$_n$-OH, was transferred to a 150 mL round bottom flask that contained 130 mL DCM/toluene (9:1 v/v). N,N′-DSC (1.84 g, 7.2 mmol) was added to the solution followed by NEt$_3$ (0.73 g, 7.2 mmol), and the reaction was maintained at room temperature overnight with magnetic stirring, in the presence of air. Thereafter, the reaction solution was extracted in a separatory funnel with 130 mL saturated aq. trisodium phosphate; the DCM phase was separated, dried with magnesium sulfate, filtered, and stripped of solvent by rotary evaporation, giving a brown oil. Subsequently, the oil was added dropwise to 5 °C Et$_2$O, resulting in a waxy brown precipitate, which was collected and dried in a vacuum oven at 40 °C for 16 h. The resulting reaction intermediate, BOC-NH-PEG$_n$-OSu, was transferred to a 100 mL round bottom flask that contained 50 mL of DCM (dried over molecular sieves). Then, Phe-OEt HCl (1.91 g, 8.3 mmol) was added, followed by NEt$_3$ (1.39 g, 13.8 mmol), and the reaction was maintained at room temperature for 16 h, with magnetic stirring in the presence of air. As above, the workup to obtain the intermediate BOC-NH-PEG$_n$-Phe-OEt was achieved by an identical method to the previous workup of the succinimide reaction, through extraction by saturated sodium phosphate, drying with magnesium sulfate, and precipitation in 5 °C Et$_2$O. The resulting waxy brown precipitate was dried at 40 °C in a vacuum oven for 16 h. Removal of the BOC protecting group from BOC-NH-PEG$_n$-Phe-OEt was conducted in a 50 mL round bottom flask by addition of 9 mL 1:4 (v/v) TFA:H_2O solution maintained at room temperature for 16 h with magnetic stirring. Then, the contents of the reaction solution were transferred

dropwise to 5 °C Et$_2$O (36 mL) which resulted in a precipitate that was separated by filtration and stripped of volatiles by rotary evaporation, yielding a waxy brown solid. Finally, in a 50 mL round bottom flask containing 3 mL of DMF (dried over molecular sieves), anhydrous glucose (0.11 g, 0.6 mmol) was added and dissolved with gentle heating. Reductive amination of glucose by reaction with NH$_2$-PEG$_n$-Phe-OEt was then carried out in the presence of NEt$_3$ (0.17 g, 1.7 mmol) and by addition of STAB-H (0.47 g, 2.2 mmol). The reaction was conducted in a 10 mL glass vial capped with a drying tube that contained CaCl$_2$, maintained at room temperature with magnetic stirring for 16 h. Once the reaction was complete, it was added dropwise into 5 °C Et$_2$O (12 mL), and the precipitate was collected and recrystallized in hot EtOH. A waxy tan solid was obtained (80 mg, 20% yield), which was dried in a vacuum oven at 40 °C for 16 h before characterization. ^{1}H NMR (600 MHz) chemical shifts (δ in ppm) in DMSO-d6/10% TFA 7.9 (s, 1H), 7.3 (dd, 5H), 4.5–2.9 (m, glucose Hs), 3.7–3.3 (m, PEG Hs), 2.2 (s, 1H), 1.1 (t, 3H); MALDI-TOF (m/z): [M + H]$^+$ calculated for $C_{20}H_{33}O_9N_2$ 445.22, found 444.99.

4.5 General procedure of protease catalyzed peptide synthesis

In a one-pot aqueous system, the grafter (e.g., Glycan-Phe-OEt, Glycan-PEG$_n$-Phe-OEt), as displayed in Figure 3 (0.54 mmol), was added to 15 mL of 0.6M PBS solution. Once dissolved, Leu-OEt HCl was added at varied amounts (0.54 mmol–5.4 mmol), in order to test the effect of grafter to monomer ratios, ranging from 1:1 to 1:10 grafter: monomer. The solution pH was adjusted to 8 with 1M NaOH and 1M HCl as needed. Papain was then added (20 mg/mL, 0.9263 U/mg, measured by azocasein assay (Brock et al., 1982; Centore et al., 2020)) and the reaction stirred for 1 h at 40°C. Reactions were worked up as described in previous studies (Centore et al., 2020).

4.6 Nuclear magnetic resonance (NMR)

^{1}H NMR, ^{13}C NMR, COSY NMR experiments were performed on a Pharaoh 600 MHz NMR in DMSO-d_6/TFA (9:1 v/v), or D$_2$O at 25°C for 32 scans (^{1}H NMR), 512 scans (^{13}C NMR), and 8–16 scans (COSY). All data was processed on Bruker TopSpin. Proton chemical shifts were referenced relative to DMSO-d_6 (2.50 ppm) or H$_2$O (4.7 ppm).

4.7 Matrix-assisted laser desorption/ ionization time-of-flight (MALDI-TOF)

MALDI-TOF was collected on a Bruker Ultraflex III MALDI-TOF/TOF in positive-ion mode. Data was acquired using FlexControl. The matrix solution consisted of 10 mg/mL of α-cyano-4-hydroxycinnamic acid (CCA) in ACN/water (1:1 v/v) with 0.1% (v/v) TFA. Samples were dissolved in the matrix solution at a concentration of 1–2 mg/mL, followed by spotting 1 μL of the sample solution onto a steel target plate. Spots were dried under a stream of air before acquiring data. The acquired data was exported as a.mzXML file and further processed on mMass and Microsoft Excel. After identifying peaks, correcting the baseline, and

smoothing the spectrum, M_n and M_w were calculated from the peak list.

4.8 Computational modeling

Computational modeling was done using PyRosetta, a Python-based interface to Rosetta. Models were scored with the ref2015 score function, with added weights for constraints to favor models with geometries that correspond to effective active sites. Chemical structures for every amino acid ester substrate were created with Avogadro and conformers for each structure were generated using the conformational generation tool in Mercury by Cambridge Crystallographic Data Centre (CCDC), which references the Cambridge Structural Database (CSD).

The papain structures were generated as previously described (Yang et al., 2020). To generate starting structures, the base crystal structure of papain from 9pap underwent a FastRelax protocol for initial minimization, while the acyl-enzyme intermediate structure from 2bu3 was used to generate constraints based on the geometry of the acyl intermediate, the nucleophilic acyl-acceptor, and the catalytic residues of papain. The acyl-donor and acyl-acceptor for each pair were docked into the active site based on the geometry of the acyl-enzyme structure from our previous models.

Models were generated via sampling of rotamers of residues and conformers of substrates to find compatible structures of the enzyme and substrates. The structures underwent two initial rounds of repack on the active site in order to resolve clashes and four rounds of minimization-and-repack on the active site to find sets of rotamers with improved favorability. Conformers for each substrate were sampled from the corresponding sets generated and rotamers of amino acids were sampled from the databases within Rosetta. Constraints were applied to ensure the sampled conformers still adhered to the necessary geometry for a catalytically active pocket. Sampling was repeated 100 times for each pair of acyl-donors and acyl-acceptors, which consists of five acyl-donors (Glucose-NH_2-Phe-OEt, Glucose-NH_2-PEG-Phe-OEt, Glucose-NH_2-PEG_2-Phe-OEt, Glucose-NH_2-PEG_3-Phe-OEt, Glucose-NH_2-PEG_4-Phe-OEt) and one acyl-acceptor (Leu-OEt). The Leu-OEt acyl-acceptor and the Glucose-NH_2-Phe-OEt acyl-donor had a set of 200 conformers, Glucose-NH_2-PEG-Phe-OEt had a set of 400, Glucose-NH_2-PEG_2-Phe-OEt had a set of 600, Glucose-NH_2-PEG_3-Phe-OEt had a set of 800, and Glucose-NH_2-PEG_4-Phe-OEt had a set of 1,000. The iterations with the lowest energies were kept for comparisons.

Data availability statement

The datasets presented in this study can be found in online repositories. The names of the repository/repositories and accession number(s) can be found below: https://figshare.com/articles/dataset/Raw_NMR_data_for_publication_doi_10_3389_fctls_2023_1275281/24514984.

Author contributions

Funding

Acknowledgments

Conflict of interest

The authors declare that the research was conducted in the absence of any commercial or financial relationships that could be construed as a potential conflict of interest.

Publisher's note

All claims expressed in this article are solely those of the authors and do not necessarily represent those of their affiliated organizations, or those of the publisher, the editors and the reviewers. Any product that may be evaluated in this article, or claim that may be made by its manufacturer, is not guaranteed or endorsed by the publisher.

Supplementary material

The Supplementary Material for this article can be found online at: https://www.frontiersin.org/articles/10.3389/fctls.2023.1275281/full#supplementary-material

References

Abdel-Magid, A. F., and Mehrman, S. J. (2006). A review on the use of sodium triacetoxyborohydride in the reductive amination of ketones and aldehydes. *Org. Process Res. Dev.* 10 (5), 971–1031. doi:10.1021/op0601013

Agarwal, A., Gupta, U., Asthana, A., and Jain, N. K. (2009). Dextran conjugated dendritic nanoconstructs as potential vectors for anti-cancer agent. *Biomaterials* 30 (21), 3588–3596. doi:10.1016/j.biomaterials.2009.03.016

Bapst, J. P., Calame, M., Tanner, H., and Eberle, A. N. (2009). Glycosylated DOTA - α-melanocyte-stimulating hormone analogues for melanoma targeting: influence of the site of glycosylation on *in vivo* biodistribution. *Bioconjug. Chem.* 20 (5), 984–993. doi:10.1021/bc900007u

Bordusa, F. (2002). Proteases in organic synthesis. *Chem. Rev.* 102 (12), 4817–4868. doi:10.1021/cr010164d

Brock, F. M., Forsberg, C. W., and Buchanan-Smith, J. G. (1982). Proteolytic activity of rumen microorganisms and effects of proteinase inhibitors. *Appl. Environ. Microbiol.* 44 (3), 561–569. doi:10.1128/aem.44.3.561-569.1982

Centore, R., Totsingan, F., Amason, A. C., Lyons, S., Zha, R. H., and Gross, R. A. (2020). Self-assembly-assisted kinetically controlled papain-catalyzed formation of mPEG-*b*-Phe(Leu)$_x$. *Biomacromolecules* 21 (2), 493–507. doi:10.1021/acs.biomac.9b01237

Deming, T. J. (2012). Ring-opening polymerization of amino acid N-carboxyanhydrides. *Polym. Sci. A Compr. Ref.* 4, 427–449. doi:10.1016/B978-0-444-53349-4.00111-4

Derakhshankhah, H., and Jafari, S. (2018). Cell penetrating peptides: A concise review with emphasis on biomedical applications. *Biomed. Pharmacother.* 108, 1090–1096. doi:10.1016/j.biopha.2018.09.097

Duro-Castano, A., Conejos-Sánchez, I., and Vicent, M. J. (2014). Peptide-based polymer therapeutics. *Polym. (Basel)* 6 (2), 515–551. doi:10.3390/polym6020515

Dutot, L., Lécorché, P., Burlina, F., Marquant, R., Point, V., Sagan, S., et al. (2010). Glycosylated cell-penetrating peptides and their conjugates to a proapoptotic peptide: preparation by click chemistry and cell viability studies. *J. Chem. Biol.* 3 (2), 51–65. doi:10.1007/s12154-009-0031-9

Erez, E., Fass, D., and Bibi, E. (2009). How intramembrane proteases bury hydrolytic reactions in the membrane. *Nature* 459 (7245), 371–378. doi:10.1038/nature08146

Fan, T., Yu, X., Shen, B., and Sun, L. (2017). Peptide self-assembled nanostructures for drug delivery applications. *J. Nanomater* 2017, 1–16. doi:10.1155/2017/4562474

Gallego, I., Rioboo, A., Reina, J. J., Díaz, B., Canales, Á., Cañada, F. J., et al. (2019). Glycosylated cell-penetrating peptides (GCPPs). *ChemBioChem* 20 (11), 1400–1409. doi:10.1002/cbic.201800720

Hadjichristidis, N., Iatrou, H., Pitsikalis, M., and Sakellariou, G. (2009). Synthesis of well-defined polypeptide-based materials via the ring-opening polymerization of α-amino acid N-carboxyanhydrides. *Chem. Rev.* 109 (11), 5528–5578. doi:10.1021/cr900049t

Jain, K., Kesharwani, P., Gupta, U., and Jain, N. K. (2012). A review of glycosylated carriers for drug delivery. *Biomaterials* 33, 4166–4186. Elsevier. doi:10.1016/j.biomaterials.2012.02.033

Kajihara, Y., Okamoto, R., Yamamoto, N., and Izumi, M. (2010). Synthesis of glycopeptides. *Methods Enzymol.* 478 (C), 503–519. doi:10.1016/S0076-6879(10)78024-1

Martin, V., Egelund, P. H. G., Johansson, H., Thordal Le Quement, S., Wojcik, F., and Sejer Pedersen, D. (2020). Greening the synthesis of peptide therapeutics: an industrial perspective. *RSC Adv.* 10 (69), 42457–42492. doi:10.1039/d0ra07204d

Moradi, S. V., Mansfeld, F. M., and Toth, I. (2013). Synthesis and *in vitro* evaluation of glycosyl derivatives of luteinizing hormone-releasing hormone (LHRH). *Bioorg. Med. Chem.* 21 (14), 4259–4265. doi:10.1016/j.bmc.2013.04.068

Pukanud, P., Peungvicha, P., and Sarisuta, N. (2009). Development of mannosylated liposomes for bioadhesive oral drug delivery via M cells of peyer's patches. *Drug Deliv.* 16 (5), 289–294. doi:10.1080/10717540902989738

Qin, X., Xie, W., Su, Q., Du, W., and Gross, R. A. (2011). Protease-catalyzed oligomerization of l -lysine ethyl ester in aqueous solution. *ACS Catal.* 1 (9), 1022–1034. doi:10.1021/cs2002884

Stawikowski, M., and Fields, G. B. (2012). Introduction to peptide synthesis. *Curr. Protoc. Protein Sci.* 1 (69), Unit 18.1–13. doi:10.1002/0471140864.ps1801s69

Viswanathan, K., Omorebokhae, R., Li, G., and Gross, R. A. (2010). Protease-catalyzed oligomerization of hydrophobic amino acid ethyl esters in homogeneous reaction media using L-phenylalanine as a model system. *Biomacromolecules* 11 (8), 2152–2160. doi:10.1021/bm100516x

Yang, F., Totsingan, F., Dolan, E., Khare, S. D., and Gross, R. A. (2020). Protease-catalyzedl-aspartate oligomerization: substrate selectivity and computational modeling. *ACS Omega* 5, 4403–4414. For Table of Contents Use Only. doi:10.1021/acsomega.9b03290

Yazawa, K., and Numata, K. (2014). Recent advances in chemoenzymatic peptide syntheses. *Molecules* 19 (9), 13755–13774. doi:10.3390/molecules190913755

Glossary

PCPS	Protease-Catalyzed Peptide Synthesis
SPPS	Solid-Phase Peptide Synthesis
NCA-ROP	N-Carboxyanhydride Ring-Opening Polymerization
Phe	Phenylalanine
Leu	Leucine
Cys	Cysteine
Gly	Glycine
Gln	Glutamine
Asp	Aspartic Acid
His	Histidine
Trp	Tryptophan
Val	Valine
Thr	Threonine
Ser	Serine
OEt	Ethyl ester
PEG	Polyethylene glycol
TFA	Trifluoroacetic acid
CHCA	α-cyano-4-hydroxycinnamic acid
DMSO-*d6*	Deuterated dimethylsulfoxide
CPP	Cell-Penetrating peptide
PPI	Poly (propylene imine)
REACH	Registration, Evaluation, Authorization and Restriction of Chemicals
AA	Amino Acid
STAB-H	Sodium triacetoxyborohydride
NMR	Nuclear Magnetic Resonance
ESI-MS	Electrospray Ionization Mass Spectrometry
MALDI-TOF	Matrix-assisted Laser Desorption/Ionization Time-of-Flight
DMF	Dimethyl Formamide
DCM	Dichloromethane
N,N′-DSC	N,N′-Disuccinimidyl carbonate
BOC	*tert*-butyloxycarbonyl